

Transport of ion beam in an annular magnetically expanding helicon double layer thruster

Yunchao Zhang, Christine Charles, and Rod Boswell

Citation: *Physics of Plasmas* (1994-present) **21**, 063511 (2014); doi: 10.1063/1.4885350

View online: <http://dx.doi.org/10.1063/1.4885350>

View Table of Contents: <http://scitation.aip.org/content/aip/journal/pop/21/6?ver=pdfcov>

Published by the [AIP Publishing](#)

Articles you may be interested in


[Ion acceleration enhanced by additional neutralizing electrons in a magnetically expanding double layer plasma](#)
Phys. Plasmas **17**, 104505 (2010); 10.1063/1.3499691


[Transport of energetic electrons in a magnetically expanding helicon double layer plasma](#)
Appl. Phys. Lett. **94**, 191503 (2009); 10.1063/1.3136721

[Xenon ion beam characterization in a helicon double layer thruster](#)
Appl. Phys. Lett. **89**, 261503 (2006); 10.1063/1.2426881


[On-axis parallel ion speeds near mechanical and magnetic apertures in a helicon plasma device](#)
Phys. Plasmas **12**, 103509 (2005); 10.1063/1.2121347

[Laboratory evidence of a supersonic ion beam generated by a current-free "helicon" double-layer](#)
Phys. Plasmas **11**, 1706 (2004); 10.1063/1.1652058

A collection of five pieces of Pfeiffer Vacuum equipment, including a red turbopump, a silver turbopump, a silver backing pump, a red turbopump with a long shaft, and a silver chamber component.

 Vacuum Solutions from a Single Source

- Turbopumps
- Backing pumps
- Leak detectors
- Measurement and analysis equipment
- Chambers and components

PFEIFFER  **VACUUM**

Transport of ion beam in an annular magnetically expanding helicon double layer thruster

Yunchao Zhang,^{a)} Christine Charles, and Rod Boswell

Space Plasma, Power and Propulsion Laboratory, Research School of Physics and Engineering,
The Australian National University, Bldg 60, Mills Road, ACT 0200, Australia

(Received 18 April 2014; accepted 11 June 2014; published online 25 June 2014)

An ion beam generated by an annular double layer has been measured in a helicon thruster, which sustains a magnetised low-pressure (5.0×10^{-4} Torr) argon plasma at a constant radio-frequency (13.56 MHz) power of 300 W. After the ion beam exits the annular structure, it merges into a solid centrally peaked structure in the diffusion chamber. As the annular ion beam moves towards the inner region in the diffusion chamber, a reversed-cone plasma wake (with a half opening angle of about 30°) is formed. This process is verified by measuring both the radial and axial distributions of the beam potential and beam current. The beam potential changes from a two-peak radial profile (maximum value ~ 30 V, minimum value ~ 22.5 V) to a flat (~ 28 V) along the axial direction; similarly, the beam current changes from a two-peak to one-peak radial profile and the maximum value decreases by half. The inward cross-magnetic-field motion of the beam ions is caused by a divergent electric field in the source. Cross-field diffusion of electrons is also observed in the inner plume and is determined as being of non-ambipolar origin. © 2014 AIP Publishing LLC. [<http://dx.doi.org/10.1063/1.4885350>]

The annular configuration of plasma sources has attracted great interests over the past few years with the classic annular configuration for Hall thrusters being widely used in the electric propulsion industry.¹ It has been suggested that preionisation for Hall thrusters would be beneficial and this could be obtained by using an annular helicon source.² A double layer generated ion beam has been experimentally shown in a cylindrical helicon thruster by Charles and Boswell.³ While small probes (<1 cm diameter) could be inserted through the center of the double layer without discernible perturbation, could an annular double layer, i.e., a robust double layer with a large inner area, exist in an annular helicon thruster? And how would the generated ion beam expand away from the annular region? This paper focuses on these questions and presents our experimental results.

The present experiment is based on the Chi Kung reactor (previously described),³ which has been modified to consist of an annular helicon source and a contiguously attached 30-cm long, 32-cm diameter, earthed aluminium diffusion chamber [Fig. 1(a)]. The annular source is constructed by inserting a 31-cm long, 5-cm diameter glass tube, sealed at the internal vacuum end, into the original Chi Kung 13.8-cm diameter glass tube. The resulting annulus has a width of 4.5 cm. A 20-cm long double-saddle antenna surrounds the outer tube in the annular region, operating at a constant radio-frequency power of 300 W at 13.56 MHz fed through a matching network. Two solenoids placed around the source (top solenoid current 0 A and exit solenoid current 9 A) generate the calculated magnetic field shown in Fig. 1(b). The field decreases from more than 300 G in the source to only a few Gauss in the diffusion chamber. Argon gas is fed to the

side wall of the diffusion chamber along with the turbomolecular pump. The base pressure and the operating gas pressure are 6.6×10^{-6} Torr and 5.0×10^{-4} Torr, measured with an ion gauge and a baratron gauge, respectively.

A source-facing retarding field energy analyser (RFEA) and an emissive probe (EP) can be mounted onto a vacuum slide on the backplate of the diffusion chamber.⁴ The slide structure allows the probes to move along both the axial and radial directions for two dimensional measurements without

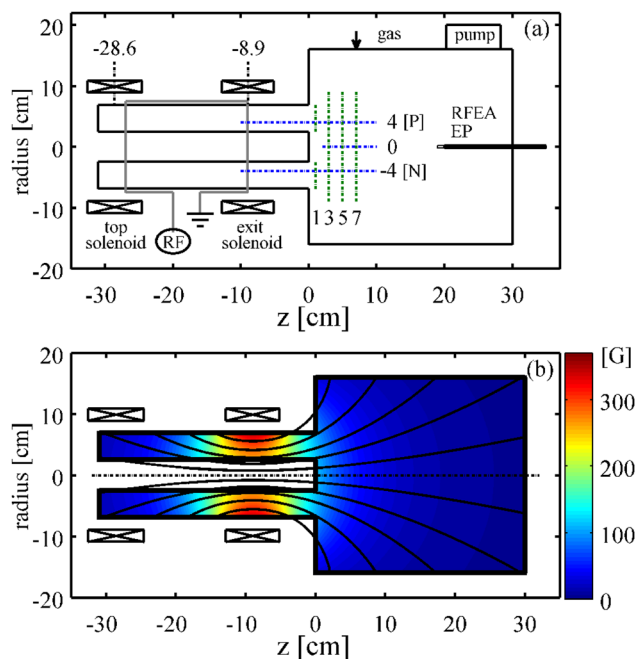


FIG. 1. (a) Annular helicon thruster, showing the major components and diagnostic probes. (b) Contour plot of the calculated magnetic field in the thruster.

^{a)}yunchao.zhang@anu.edu.au

breaking the vacuum (except when changing the probe). The probe shaft and diffusion chamber are grounded and connected to the clean earth of the building similarly to the previous ion beam experiment investigation for the helicon double layer thruster.^{3,5} In the latter configuration, it was shown that immersing the helicon double layer thruster in a 1.4-m long, 1-m diameter space-simulation vacuum chamber did not affect the existence of the ion beam.⁶ In this experiment, an energy analyser consisting of four grids and a collector plate is used.⁷ The RFEA measures the collector current versus discriminator voltage characteristics $I(V_d)$ and from the corresponding derivative, the ion energy distribution function (IEDF) can be obtained. The $I(V_d)$ curve gives the total ion current $I(V_d = 0 \text{ V})$ and beam current $I(V_d = V_b)$. The IEDF is modelled by a sum of one to three Gaussians and determines the plasma potential and beam potential. The EP is used to measure the local plasma potential with the floating potential method. It eliminates the sheath around the tungsten wire by emitting electrons, and pushes the probe floating potential to equal the plasma potential. The EP can also be used as a Langmuir probe (no emitting current) to define the ion saturation current at a negative bias voltage from the $I(V)$ curve.⁸ For the present experiment, the energy resolution of the RFEA is expected to be less than 1 eV.⁹ A heating current between 2.6 A and 2.8 A is applied for the EP to reach the floating potential saturation, resulting in a voltage drop of about 2.3 V across the tungsten filament; hence, the plasma potential measurement from the EP has an uncertainty of $\pm 1.2 \text{ V}$.¹⁰ The experimental uncertainty in the total ion current measured by the RFEA and the ion saturation current measured by the EP is estimated at $\pm 15\%$ from repeating the measurements multiple times.

The plasma in the source is formed between the walls of the inner closed cylinder and the outer tube [Fig. 1] and operates in an inductive mode similarly to the experiment previously reported for the cylindrical helicon double layer thruster.⁵ It is a low-pressure weakly collisional discharge with an ion-neutral mean free path of $\lambda_i \sim 6 \text{ cm}$ comparable with the radial characteristic size of the source (annulus width of 4.5 cm). Fig. 2(a) presents the axial EP measurement of the plasma potential along $r = -4 \text{ cm}$ and $r = 4 \text{ cm}$, showing a high potential of 30–35 V in the source decreasing to 18–20 V in the diffusion chamber. A source-facing RFEA mounted through the side wall of the diffusion chamber is used as a witness probe to detect whether the EP positioned in the source dramatically perturbs the plasma or not. The results from the witness probe keep constant when the EP moves from the source into the diffusion chamber, showing that the presence of the EP in the source has little influence on the plasma and the EP gives reliable measurements. Measurements from the EP are in good agreement with the RFEA, showing the symmetry of the annular thruster, and suggesting a stable, 5-cm wide double layer;¹¹ the beam potential ($\sim 30 \text{ V}$) measured by the RFEA is detected from $z = 1 \text{ cm}$ and is consistent with the upstream plasma potential measured by the EP in the source; the plasma potentials measured by the two probes in the diffusion chamber are also in good agreement. The high plasma potential and negative floating potential in the source region indicate that hot

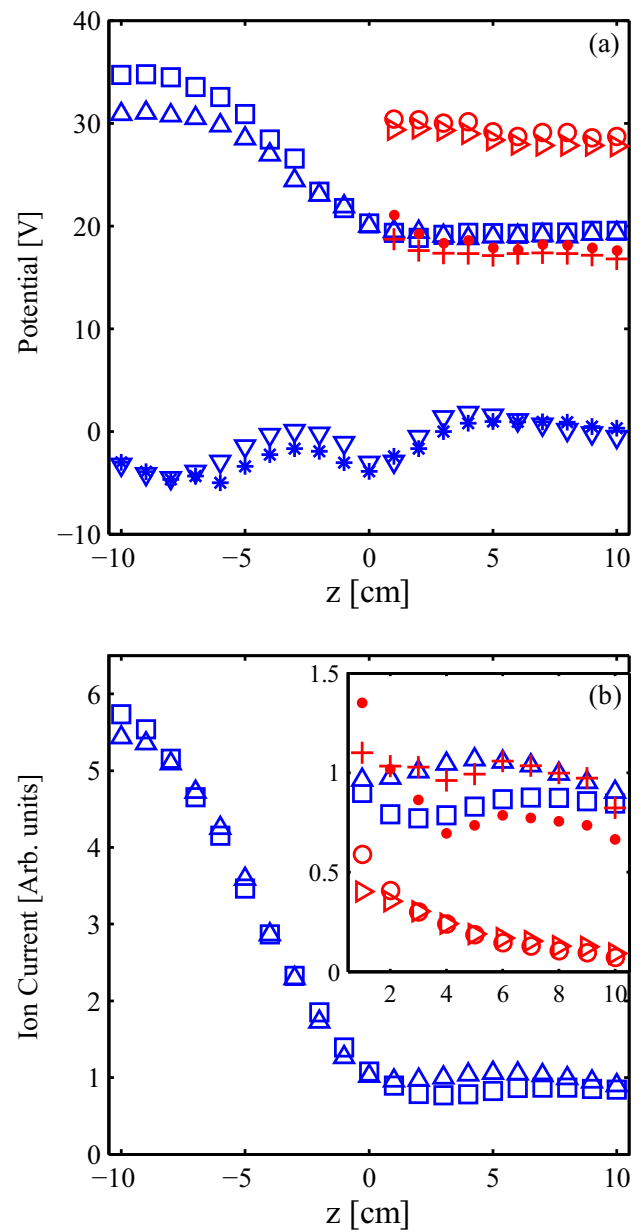


FIG. 2. For simplicity, N and P are used to represent the axial measurements along $r = -4 \text{ cm}$ (negative) and $r = 4 \text{ cm}$ (positive), respectively, as shown in Fig. 1. (a) Axial plasma potential measured by EP (Δ [N], \square [P]), RFEA ($+$ [N], \bullet [P]), floating potential measured by EP ($*$ [N], ∇ [P]) and beam potential measured by RFEA (\triangleright [N], \triangleleft [P]). (b) Axial ion saturation current measured by EP (Δ [N], \square [P]), total ion current measured by RFEA ($+$ [N], \bullet [P]) and beam current measured by RFEA (\triangleright [N], \triangleleft [P]); the inset in (b) is a zoomed figure for the range of $z = 1 \text{ cm}$ to 10 cm .

electrons are bounded and repelled by the double layer.¹² The total ion current and beam current of the RFEA $I(V_d)$ curve are determined as $I(0 \text{ V})$ and $I(30 \text{ V})$, respectively,³ while the ion saturation current from the EP is determined with an applied bias voltage of -80 V as a Langmuir probe.⁸ The ion currents along $r = -4 \text{ cm}$ and $r = 4 \text{ cm}$, including the ion saturation current from the EP and the total ion current and beam current from the RFEA, are scaled for comparison as they are collected from two different probes [Fig. 2(b)]. The formulae for the scaling are given below and since the RFEA measurements range from $z = 1 \text{ cm}$ to 10 cm , the mean value of ion currents in this range can be used as the

denominator for the scaled ion current to form a ratio parameter. For the ion saturation current,

$$\hat{I}_{sat} = \frac{I_{sat,r}}{\langle I_{sat,r=-4} \rangle_{z=1 \rightarrow 10}}, \quad (1)$$

for the total ion current and beam current,

$$\hat{I}_{tot} = \frac{I_{tot,r}}{\langle I_{tot,r=-4} \rangle_{z=1 \rightarrow 10}}, \quad \hat{I}_{beam} = \frac{I_{beam,r}}{\langle I_{tot,r=-4} \rangle_{z=1 \rightarrow 10}}. \quad (2)$$

Fig. 2(b) presents the ion saturation current decreasing from the source into the diffusion chamber after passing through the throat of the magnetic nozzle at $z \approx -10$ cm, where the magnetic field is strongest and the ion current peaks. In the inset of Fig. 2(b), the total ion current from the RFEA gives consistent results with the ion saturation current from the EP (no emitting current). Their profiles show a slight dip at $z \approx 3$ cm, and the dip is also observed in other double layer experiments.¹³ The beam current decreases axially due to ion-neutral charge exchange collisions.

Figs. 3(a) and 3(b) show the radial profiles of the beam potential and beam current (measured by the RFEA) for an increasing axial positions at every 2 cm from $z = 1$ cm to 7 cm. The radial profile of the beam potential in Fig. 3(a) shows that, along the axial direction, the two peaks gradually decrease while the center segment gradually increases until the profile becomes flat at $z = 7$ cm. The beam potential profile changes from a two-peak distribution with maximum value ~ 30 V, minimum value ~ 22.5 V to a flat distribution of ~ 28 V as the ion beam propagates from the annular source into the diffusion chamber. The radial profile of the beam current in Fig. 3(b) exhibits a similar behaviour along the axial direction: the two peaks of the beam current profile gradually decrease and disappear while the center segment increases in magnitude and the whole changes from a concave shape to a convex shape. The beam current profile changes from a two-peak distribution to a one-peak distribution, indicating that a plasma wake exists downstream of the inner closed cylinder and the wake is gradually filled along the axial direction. The maximum value of the beam current profile at $z = 7$ cm is half of that at $z = 1$ cm and the average level of the beam current also decreases axially due to charge exchange collisions. The boundary of the ion beam and the wake geometry is presently characterised by the threshold current integration method

$$\eta = \frac{\int_{-R}^R f[I_{beam}(r)] dr}{\int_{-R}^R I_{beam}(r) dr}, \quad (3)$$

$$f[I_{beam}(r)] = \begin{cases} I_{beam}(r) & I_{beam}(r) \geq I^* \\ 0 & I_{beam}(r) < I^*. \end{cases} \quad (4)$$

The boundary of the ion beam is determined by $I_{beam}(r) = I^*$ and the threshold current I^* can be solved once the integration percentage η is set. This procedure is similar to the idea of Lebesgue integration: the integration

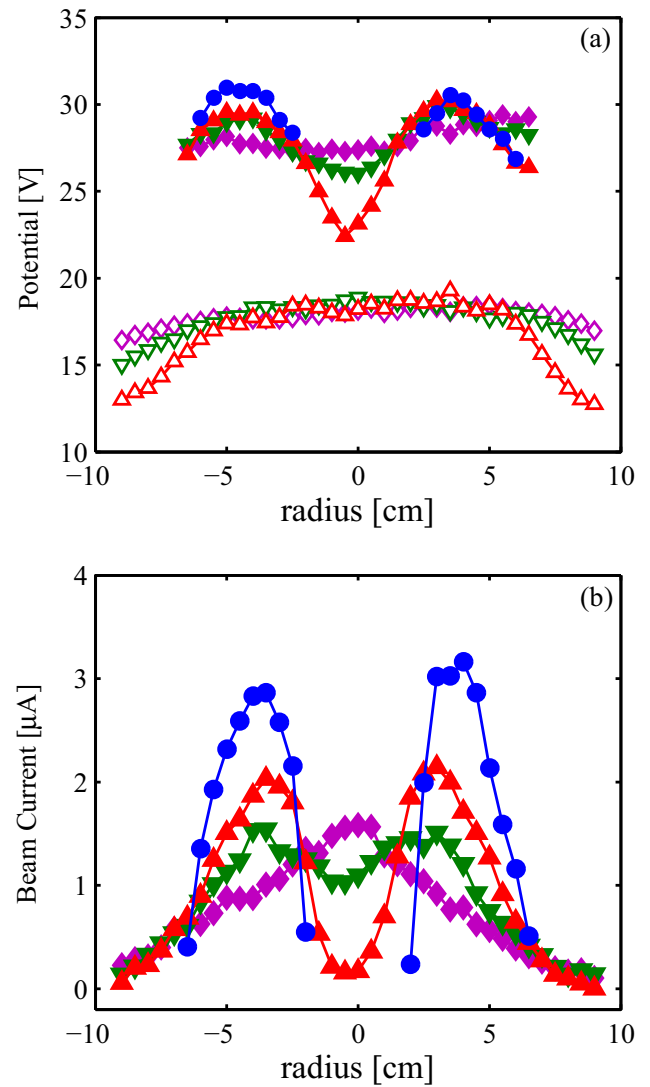


FIG. 3. (a) Radial potential measurement (solid markers for beam potential and open markers for plasma potential) and (b) radial beam current measurement along $z = 1$ cm (\circ), $z = 3$ cm (Δ), $z = 5$ cm (∇), and $z = 7$ cm (\diamond), respectively, measured with the RFEA.

percentage η accounts for the contribution of the beam current from maximum to minimum. For a given η , the ion beam is defined by the highest beam current regions, which fits the main body of the radial beam distribution. Fig. 3(b) shows a good symmetry of the beam current distribution. Fig. 4 shows the negative side of the radius [Fig. 1] and the boundary of the annular ion beam derived from this method. The inner edges of the annular ion beam (from $r = -2.5$ cm, $z = 1$ cm) move inward along the axial direction and merge on the central axis ($r = 0$ cm), showing that the beam ions from the annular aperture converge into the central region downstream of the source. The ion beam changes to a solid structure after the wake region, which is identified to be a reversed cone with a half opening angle of about 30° . When η decreases, the outer boundary shrinks, while the inner boundary broadens, making the beam into a thinner annulus. The inward motion of the ion beam is more clearly seen than the outward divergence of the ion beam (the outward divergence of an ion beam in a cylindrical system has been

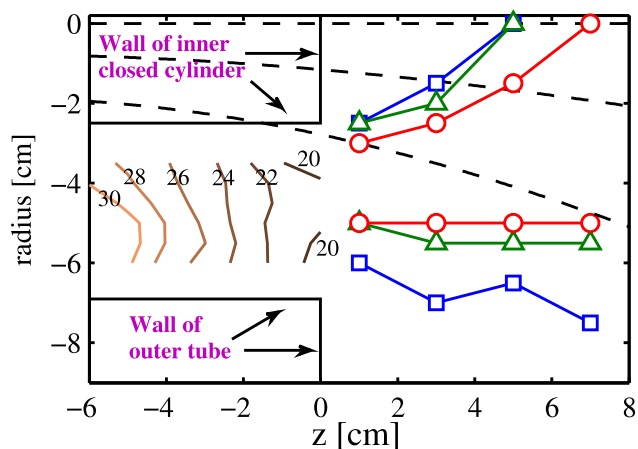


FIG. 4. Bottom half of the system (negative radius) showing the boundary of the annular ion beam with the integration percentages of 90% (\square), 75% (\triangle), and 60% (\circ). Contours of plasma potential are shown in the annular source region. The magnetic field lines are represented by the dashed lines.

studied by Cox *et al.*⁵). If the ion beams were only influenced by the Lorentz force, its trajectory would not move towards the central region, and the axial component of the velocity would remain dominant.¹⁴ For the magnetic field shown in Fig. 1(b), its effect on the ions mainly occurs in the source region with a Larmor radius $r_{ci} < 1$ cm. As the magnetic field decreases in the diffusion chamber, the Larmor radius rapidly increases to the level of the ion-neutral mean free path and of the chamber length further out. Hence, the magnetic field would have a relatively weak effect on the ion motion in the diffusion chamber.

The potential (the beam potential and plasma potential measured by the RFEA, the plasma potential measured by the EP) and the ion current (the beam current and total ion current measured by the RFEA, the ion saturation current measured by the EP) along the central z-axis ($r = 0$ cm) are shown in Fig. 5. The ion current is scaled using the same method as Eqs. (1) and (2) except for a denominator being the mean value along z-axis. Collision¹⁵ and plasma expansion¹⁶ are not considered to be key factors contributing to the merging of the annular ion beam at $z \approx 6$ cm in the central region. If ion collisions dominate in the inner region of the plume and yield an inward motion of the ion beam, the beam potential should decrease along z-axis as the ions suffer more collisions and lose beam energy. However, Fig. 5(a) shows that the beam potential increases along the z-axis until it matches the beam potential along $r = -4$ cm and $r = 4$ cm [Fig. 2(a)] at $z \approx 6$ cm. The momentum equation in the plasma expansion model is based on ambipolar diffusion with an electric field, but in the present system the radial distribution of the plasma potential is flat in the central region of the diffusion chamber [Fig. 3(a)] showing small or no radial electric field. Hence, the plasma potential distribution in the source is thought to be the main effect contributing to the inward motion of the ion beam. A divergent electric field is identified in the annular source from the potential contours shown in Fig. 4. The field region near the inner closed cylinder (-5 cm $< r < -2.5$ cm) has an inward component, which will accelerate the beam ions towards the central region downstream of the source. The beam current shows a vaulted

profile that increases between $z = 2$ cm and 6 cm and then decreases, displaying a different behaviour from that along $r = -4$ cm and $r = 4$ cm with a monotonic decrease as shown in the inset of Fig. 2(b). The increasing segment corresponds to the transfer region between the wake and the solid ion beam. The location ($z = 6$ cm, $r = 0$ cm) where the beam current is maximum approximately determines the edge of the wake shown in Fig. 5(b), which is in agreement with the beam merging location in Fig. 4.

Electrons are well confined by the expanded magnetic field line from the source into the diffusion chamber with a gyration radius $r_{ce} < 1$ mm. The electrons within the wake have a lower energy compared with the electrons outside the wake, which is deduced from two experiments: first, the

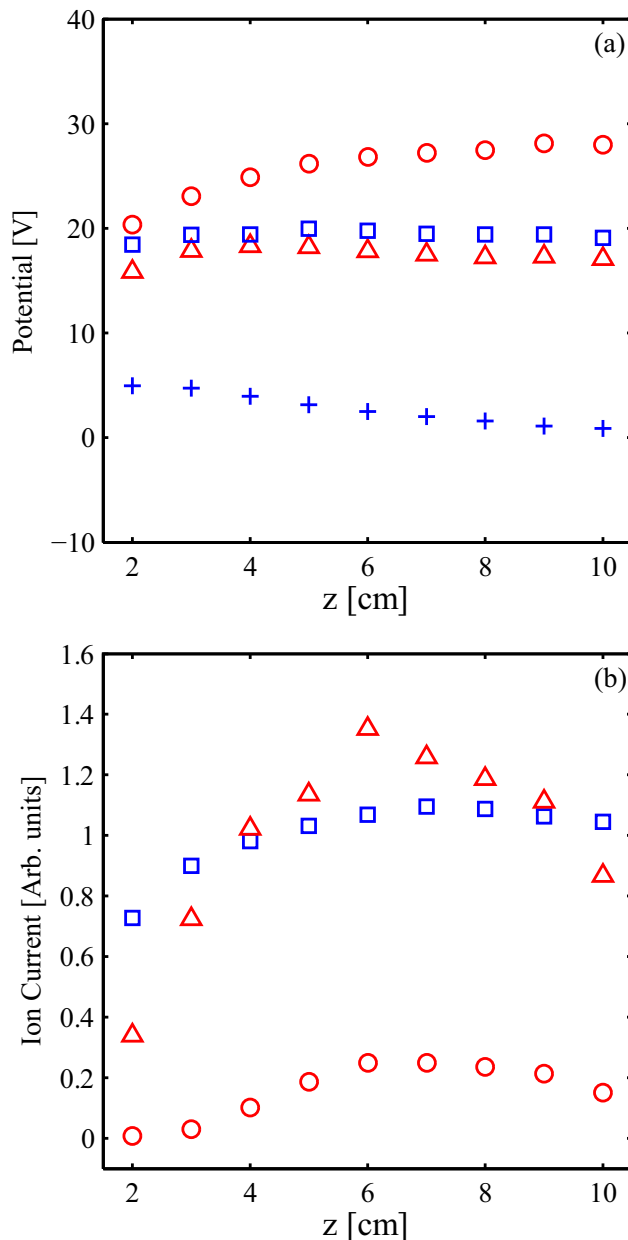


FIG. 5. (a) Axial plasma potential along the z-axis ($r = 0$ cm) measured by EP (\square), RFEA (\triangle), floating potential measured by EP (+) and beam potential measured by RFEA (\circ). (b) Axial ion saturation current measured by EP (\square), total ion current measured by RFEA (\triangle) and beam current measured by RFEA (\circ).

difference between the measured plasma potential and floating potential is theoretically estimated to be $5.2T_e$. In both Figs. 4 and 5, the plasma potential measured by the RFEA shows a good agreement with that measured by the EP, and the plasma potential keeps a mean value of 19 V with a small variance. The floating potential along the z-axis ($r=0$ cm) is higher than the floating potential along $r=-4$ cm and $r=4$ cm in the axial wake range ($0\text{ cm} < z < 6\text{ cm}$, $r=0$ cm), with a maximum difference about 5 V at $z=2$ cm and 3 cm [Fig. 5]. Hence, the electron temperature at $z=3$ cm, $r=-4$ cm is about 1 eV higher than that at $z=3$ cm, $r=0$ cm (within the wake). The difference between the plasma potential and floating potential at $z=3$ cm, $r=0$ cm is about 15 V, so the electron temperature will be 3 eV. Second, analysis of the $I(V)$ curve¹⁷ measured with the EP yields an electron temperature of 2.7 eV at $z=3$ cm, $r=0$ cm (within the wake) and 3.7 eV at $z=3$ cm, $r=-4$ cm (out of the wake). The results of the two experiments are in good agreement, showing that a relatively cold electron population exists in the wake region. The electrons must experience a cross-field diffusion to enter the inner plume region. The cross-field diffusion is identified to be a non-ambipolar diffusion¹⁸ from the flat radial distribution of plasma potential shown in Fig. 3(a). Further study is required to determine the mechanism of this diffusion such as the electron collisions or the eddy current effects.¹⁵

In summary, a robust annular double layer which generates an annular ion beam has been measured in a helicon thruster. The ion beam diverges to form a solid structure in the inner plume as well as a plasma wake. Cross-field motion of ions and electrons is observed in the plasma plume. It is difficult to do a complete analytical model for the cross-field motion in the system; however, our experimental results make some contributions to understand this physical procedure. The cross-field motion of ions is thought to be dominated by the potential distribution in the source, not by ambipolar diffusion or collisions. The cross-field diffusion of electrons is identified to be non-ambipolar but the related mechanism is still unclear.

- ¹D. M. Goebel and I. Katz, *Fundamentals of Electric Propulsion: Ion and Hall Thrusters*, JPL Space Science and Technology Series, edited by J. H. Yuen (John Wiley & Sons, 2008).
- ²M. Yano and M. L. Walker, "Plasma ionization by annularly bounded helicon waves," *Phys. Plasmas* **13**, 063501 (2006).
- ³C. Charles and R. W. Boswell, "Laboratory evidence of a supersonic ion beam generated by a current-free helicon double-layer," *Phys. Plasmas* **11**, 1706 (2004).
- ⁴W. Cox, C. Charles, and R. W. Boswell, "Magnetic ion beam deflection in the helicon double-layer thruster," *J. Propul. Power* **26**, 1045 (2010).
- ⁵W. Cox, C. Charles, R. W. Boswell, and R. Hawkins, "Spatial retarding field energy analyzer measurements downstream of a helicon double layer thruster," *Appl. Phys. Lett.* **93**, 071505 (2008).
- ⁶M. D. West, C. Charles, and R. W. Boswell, "Testing a helicon double layer thruster immersed in a space-simulation chamber," *J. Propul. Power* **24**, 134 (2008).
- ⁷G. D. Conway, A. J. Perry, and R. W. Boswell, "Evolution of ion and electron energy distributions in pulsed helicon plasma discharges," *Plasma Sources Sci. Technol.* **7**, 337 (1998).
- ⁸J. P. Sheehan and N. Hershkovitz, "Emissive probes," *Plasma Sources Sci. Technol.* **20**, 063001 (2011).
- ⁹C. Charles, A. W. Degeling, T. E. Sheridan, J. H. Harris, M. A. Lieberman, and R. W. Boswell, "Absolute measurements and modeling of radio frequency electric fields using a retarding field energy analyzer," *Phys. Plasmas* **7**, 5232 (2000).
- ¹⁰T. Lafleur, C. Charles, and R. W. Boswell, "Detailed plasma potential measurements in a radio-frequency expanding plasma obtained from various electrostatic probes," *Phys. Plasmas* **16**, 044510 (2009).
- ¹¹N. Hershkovitz, "Sheaths: More complicated than you think," *Phys. Plasmas* **12**, 055502 (2005).
- ¹²K. Takahashi, C. Charles, R. Boswell, W. Cox, and R. Hatakeyama, "Transport of energetic electrons in a magnetically expanding helicon double layer plasma," *Appl. Phys. Lett.* **94**, 191503 (2009).
- ¹³C. Charles and R. Boswell, "Current-free double-layer formation in a high-density helicon discharge," *Appl. Phys. Lett.* **82**, 1356 (2003).
- ¹⁴F. N. Gesto, B. D. Blackwell, C. Charles, and R. W. Boswell, "Ion detachment in the helicon double-layer thruster exhaust beam," *J. Propul. Power* **22**, 24 (2006).
- ¹⁵A. P. Zhilinskii and L. D. Tsengin, "Collisional diffusion of a partially-ionized plasma in a magnetic field," *Sov. Phys. Usp.* **23**, 331 (1980).
- ¹⁶J. Tao, K. Beardsley, A. Seyhonzadeh, K. Tai, P. Forsling, and K. E. Lonngren, "Plasma flow characteristics through small orifices," *J. Appl. Phys.* **65**, 4192 (1989).
- ¹⁷N. Hershkovitz, "How Langmuir probes work," in *Plasma Diagnostics, Plasma-Materials Interactions Vol. 1*, edited by O. Auciello and D. L. Flamm (Academic Press, Inc., 1989), Chap. 3, p. 113.
- ¹⁸A. Fruchtman, "Ambipolar and nonambipolar cross-field diffusions," *Plasma Sources Sci. Technol.* **18**, 025033 (2009).